Manuscript prepared for Atmos. Chem. Phys.
with version 2014/09/16 7.15 Copernicus papers of the LaTeX class copernicus.cls.
Date: 17 May 2016

Characteristics of "brown" aerosol in the urban Po Valley atmosphere

F. Costabile[1], S. Gilardoni[2], F. Barnaba[1], A. Di Ianni[1], L. Di Liberto[1], D. Dionisi[1], M. Manigrasso[3], M. Paglione[2], V. Poluzzi[4], M. Rinaldi[2], M.C. Facchini[2], and G. P. Gobbi[1]

[1]Institute for Atmospheric Sciences and Climate (ISAC), National Research Council (CNR), Rome, Italy
[2]Institute for Atmospheric Sciences and Climate (ISAC), National Research Council (CNR), Bologna, Italy
[3]INAIL, Rome, Italy
[4]ARPA ER, Bologna, Italy

Correspondence to: F. Costabile (f.costabile@isac.cnr.it)

Abstract. We characterized the nondust aerosol having the strongest spectral dependance of light absorption (as indicated by the Absorption Ångström Exponent, AAE) at visible wavelengths in the urban ambient atmosphere of the Po Valley (Bologna). We defined "brown" this bulk aerosol with brown color (it does not necessarily equate to brown carbon). In situ ground measurements of aerosol spectral optical properties, PM_1 chemical composition (HR-ToF-AMS), and coarse and fine size distributions, were carried out in Bologna, and data statistically analysed. Findings prove that "brown" aerosol is a secondary aerosol with AAE values from 2.5 to 6, containing large concentrations of organic aerosol (OA) in the larger accumulation mode particles previously referred to as droplet mode particles. Nitrate is an additional likely component. Its spectral optical signature, and possible sources, are investigated. To our knowledge, no previous work has considered these issues in the ambient atmosphere. We compared to literature to put findings in a broader perspective. There is consistency with recent "diluted" urban observations (airborne, and AERONET), and combustion chamber observations. Our study adds to these previous ones that the high AAE values featuring the "brown" aerosol depend on the OA to Black Carbon (BC) ratio more than on OA, and that the link between AAE and OA-to-BC (already observed for freshly emitted primary aerosols from biomass burning) does exist in the ambient atmosphere for this aged "brown" aerosol, as well. The comparison with studies on the composition evolution of OA in the atmosphere strengthens the result that this "brown" aerosol contains aged OA, and give insights into aged brown OA formation processes. Findings will have important atmospheric implications for modeling studies, and remote sensing observations, as regards parametrization and identification of brown OA, and brown carbon in the atmosphere.

1 Introduction

Aerosol has an important role in the Earth's climate with both direct and indirect effects; beside that, it affects air quality and atmospheric chemistry. At present, our understanding of the light-absorbing aerosol types is very incomplete (see reviews by Laskin et al., 2015; Moise et al., 2015) An important absorber of solar radiation in the visible region is the atmospheric carbonaceous aerosol (IPCC 2013). In the classification of its components proposed by poschl2003, visible-light absorbing properties were varied between two extremes. On one side, there is Black Carbon (BC), refractory material that strongly absorbs light over a broad spectral range. On the other side, there is the colourless Organic Carbon (OC), non-refractory material, with no absorption or little absorption in the UV spectral range. There is a gradual decrease of thermochemical refractiveness and specific optical absorption going from BC graphite-like structures to non-refractive and colorless OC. Also, there is a gradual decrease in the volatility from BC (the lowest volatility), to colorless non-refractory volatile OC (the highest volatility). A broad range of coloured organic compounds, with volatility in between these two extremes, have recently emerged in the scientific literature for their possible role in the Earth's climate. The term "brown carbon" (BrC) has emerged to describe this aerosol having an absorption spectrum smoothly increasing from the vis to the near-UV wavelengths, with a strong wavelength dependance of the light absorption coefficient ($\lambda^{-2} - \lambda^{-6}$) (Andreae and Gelencsér, 2006; Moosmüller et al., 2011; Bond et al., 2013; Laskin et al., 2015; Moise et al., 2015). In fact, BrC lacks a formal analytical definition (Bond et al., 2013). In this study, we will refer to a "brown" aerosol to indicate an aerosol type with high values (2-6) of the Absorption Ångström Exponent (AAE), a parameter describing the wavelength (λ) dependent absorption coefficient (σ_a) of light by aerosol, written as:

$AAE(\lambda) = -\frac{dln(\sigma_a)}{dln(\lambda)}$.

What is known about the BrC aerosol is that it is an organic matter having both primary and secondary sources (Laskin et al., 2015). Primary BrC can be emitted together with BC from low-temperature combustion processes, like wood combustion (Andreae and Gelencsér, 2006). Secondary organic aerosol (SOA) formed in the atmosphere contributes to the light absorbing carbon, as well (Moise et al., 2015, and references therein), but only a few works have analysed the secondary brown carbon associated to SOA (Saleh et al., 2013; Zhang et al., 2013, 2011).

Numerous evidences indicate increased absorption towards UV for aerosol particles having high nitrate (e.g., Zhang et al., 2013; Jacobson, 1999) and sulfate contents (Powelson et al., 2014; Lin et al., 2014; Lee et al., 2013; Song et al., 2013). Lin et al. (2014) reported the formation of light-absorbing SOA constituents from reactive uptake of isoprene epoxydiols onto preexisting acidified sulfate seed aerosol as a potential source of secondary BrC under tropospheric conditions. Powelson et al. (2014) discussed the BrC formation by aqueous-phase carbonyl compound reactions with amines and ammonium sulfate. Lee et al. (2013) studied the likely and unkown effect of sulfate on the formation of light absorbing materials and organo-nitrogen via aqueous glyoxal chemistry

in aerosol particles. Song et al. (2013) observed significant light absorption at 355 and 405 nm for the SOA formed from an α-pinene + O_3 + NO_3 system only in the presence of highly acidic sulfate seed aerosols under dry conditions. Several studies demonstrated the importance of ammonium, both as a catalyst and as a reactant, in the formation of light-absorbing products (Laskin et al., 2015; Powelson et al., 2014). SOA formation can occur both in the gas and condensed phase. Recently, an efficient SOA production has been recognised in cloud/fog drops and water containing aerosol: water soluble products of gas phase photochemical reactions may dissolve into an aerosol aqueous phase and form SOA through further oxidation, this SOA being referred to "aqSOA" (Ervens et al., 2011; Laskin et al., 2015). AqSOA formation impacts total SOA mass, and aerosol size distributions by adding mass to the so-called "droplet mode" (Ervens et al., 2011). Meng and Seinfield (1994) showed that the aerosol "droplet mode" in urban areas is the result of activation of smaller particles to form fog, followed by aqueous-phase chemistry, and fog evaporation. It was demonstrated that aqSOA formation can affect aerosol optical properties by adding light-absorbing organic material at UV wavelengths (Shapiro et al., 2009; Ervens et al., 2011).

Despite the efforts made, relations between optical properties and chemical composition of organic compounds with spectrally variable light absorption (high AAE) are poorly understood (Laskin et al., 2015). A number of previous works (Shinozuka et al, 2009; Russell et al., 2010; Arola et al., 2011) studied how the organic aerosol (OA) mass fraction (f_{OA}) relates to AAE, and to Single Scattering Albedo (SSA), the ratio of scattering to extinction, a key parameter to understand aerosol warming or cooling effect. Results from in situ measurements on the C-130 aircraft mostly over Central Mexico during MILAGRO (Russell et al., 2010) showed that both Organics and dust increase AAE values. Russell et al. (2010) showed a direct correlation between AAE and f_{OA}, the larger particles (dust) having higher AAE, and the smaller particles (pollution related) having lower AAE. On the basis of the same data, Shinozuka et al (2009) showed that AAE generally increases as f_{OA} or SSA increases. This was explained by the presence of humic like substances (HULIS) and dust, which are colored (high AAE), weak absorbers (high SSA), with high f_{OA}. Very recently, Saleh et al. (2014) burnt a selection of biomasses in a combustion chamber, varying the combustion parameters to obtain a range of BC-to-OA ratios. This ratio, the relative proportions of BC and OA mass, depends on fire characteristics, and determine its colour from black to brown to white as the ratio decreases (Bellouin , 2014). Their findings link the extent of absorbance to the BC-to-OA ratio for aged and fresh biomass burning aerosols. If confirmed by further studies, this link can be a potentially strong predictive tool for light-absorbing properties of biomass burning aerosols (Bellouin , 2014; Moise et al., 2015). Following the approach of Saleh et al. (2014), Lu et al. (2015) reviewed available emission measurements of biomass burning and biofuel combustion, and found similar results indicating that AAE of the bulk OA decreases with the BC-to-OA ratio. They conclude that the absorptive properties of OA from biomass/ biofuel burning depend strongly on burning conditions and weakly on fuel types and atmospheric processing.

In this study, we characterize the nondust aerosol having the strongest spectral dependance of light absorption (as indicated by the AAE) at visible wavelengths in the ambient atmosphere. In situ ground ambient measurements of chemical (HR-ToF-AMS), optical (3-λ nephelometer and PSAP), and micro-physical (SMPS and APS) aerosol properties were taken in Bologna, Po Valley, together with ancillary observations (including ceilometer retrievals). Major features of the "brown" aerosol in the ambient urban atmosphere are investigated. We used a global approach where the aerosol type, as a whole, is linked to the highest AAE values. We investigate sources of this brown aerosol by relating AAE to primary and secondary aerosol populations extracted through a statistical analysis of size distribution, and mass spectral features. We then characterise physico-chemical properties of the observed brown aerosol, and illustrate a case-study. Findings are then discussed in comparison with previous literature works to explore their general validity instead of treating them like results of a local study.

2 Experimental

Optical, chemical, and microphysical aerosol properties were measured, in the framework of the ARPA ER Supersite project, at the urban background site of Bologna (44 ° 31' 29" lat, 11° 20' 27' lon), in the Po Valley (Italy). Two measurement campaigns lasting one month were taken: October 22 - November 13, 2012 (Fall campaign), and February 1-27, 2013 (Winter campaign). Measurements performed are detailed below.

2.1 Measurement cabins and sampling lines

Equipment was set up in two different cabins, located side by side. Optical properties and coarse fraction size distributions were measured in the same cabin, all the instruments set-up on the same inlet system equipped with a PM_{10} head. External air was pumped in the cabin into a stainless steel tube (length = 4.0 m) by an external pump ensuring a laminar flow (Reynolds number <2000). The cabin was conditioned at 20-25°C. The difference between air temperature and dew point was enough to dry sampled air. Chemical properties and fine and ultrafine particle number size distribution were measured through a separate stainless steel inlet tube equipped with a PM_1 head.

2.2 Optical Measurements

Spectral optical properties in the visible range were measured online with a 5 minute time resolution. Dry aerosol absorption coefficients, $\sigma_a(\lambda)$, at three wavelengths (λ = 467, 530, 660 nm) were measured by a 3-wavelength particle soot absorption photometer (PSAP, Radiance Research), together with dry aerosol scattering coefficients ($\sigma_s(\lambda)$) at 450, 525, and 635 nm, by an integrating nephelometer (Ecotech, mod. Aurora 3000). Like all filter based methods, PSAP suffers from a number of measurement artifacts, including an overestimate of absorption if light absorption is also

affected by particulate light scattering, and a dependance of measurements on filter transmittance (Tr). There are in literature correction algoriths developed to overcome these artifacts - Lack et al. (2008); Virkkula (2010); Backman et al. (2014) Bond et al. (1999), and the comprehensive review by Bond et al. (2013). We corrected raw PSAP data after the iterative procedure finally described by Virkkula (2010), where only data with Tr >0.7 were retained. The wavelength-resolved $\sigma_s(\lambda)$ necessary to correct PSAP raw data were taken from nephelometer data corrected for truncation (Anderson and Ogren (1998), Bond (2001), and Müller et al., 2011). The scattering error after the truncation error correction is $\frac{\delta(\sigma_s)}{\sigma_s}$ = 0.02 (Bond et al., 2013). The uncertainty of $\sigma_a(\lambda)$ derived from PSAP data after these corrections has been estimated to be $\frac{\delta(\sigma_a)}{\sigma_a}$ = 0.2 (Virkkula, 2010; Lack et al., 2008; Bond et al., 1999; Virkkula, 2010; Cappa et al., 2008). These PSAP-derived $\sigma_a(\lambda)$ can be considered an upper limit of the "true" value (Subramanian et al., 2007; Lack et al., 2008).

After all corrections, data were checked (by visual inspection) to find any outlier/low values that could significantly influence data statistics. These values can be due to variability in the measurements or to experimental errors. According to manufacturers: (i) PSAP sensitivity is <1 Mm^{-1}, and measurement range is 0-50 Mm^{-1}; (ii) the lower detectable limit of the nephelometer is 0.3 Mm^{-1}, with calibration tolerance of $\pm$ 4 Mm^{-1}, and measurement range 0-2000 Mm^{-1}. A few data (124 records having σ_a <1 Mm^{-1}, less than 20 records with σ_s <10 Mm^{-1}, and some points with σ_s >700 Mm^{-1}) were discarded, as they were considered dubious values (comparing to data variability during the field, illustrated in the Supplementary material).

2.3 Chemical Measurements

Chemical composition of atmospheric aerosol particles were characterized online with a High Resolution Time of Flight Aerosol Mass Spectrometer (HR-ToF-AMS, Aerodyne Research Inc., Billerica) (DeCarlo et al., 2006). The HR-ToF-AMS measured the chemical composition of non-refractory PM_1 (nr-PM_1), i.e sulfate, nitrate, ammonium, chloride, and organic aerosol. The instrument alternated acquisition in V-mode (higher sensitivity and lower mass spectral resolution), and W mode (lower sensitivity and higher mass spectral resolution) every 2.5 minutes. Quantitative information discussed here corresponds to the data collected in V mode. While operating in the V mode, the instrument measures particle size distribution based on their time of flight (Jimenez et al., 2003). HR-ToF-AMS data were analyzed using SQUIRRELL v1.51 and PIKA v1.10 software (D. Sueper, University of Colorado, Boulder, Boulder, CO, USA) within Igor Pro 6.2.1 (WaveMetrics, Lake Oswego, OR). Collection efficiency was calculated according to Middlebrook et al. (2012) based on aerosol chemical composition, and relative humidity. Data validation was performed by comparison with offline measurements of sulfate, ammonium, and nitrate concentrations in PM_1 aerosol samples. The HR-ToF-AMS aerosol sample line was dried below 40% RH with a Nafion drier. The uncertainty of the AMS-derived OA was assumed to be $\frac{\delta(OA)}{OA}$ = 0.2 according to Quinn (2008).

2.4 Particle Number Size distributions

Particle number size distributions (PNSDs) were measured by combining a commercial Scanning Mobility Particle Sizer (SMPS, TSI mod. 3080 with Long-DMA, TSI mod. 3081, equipped with a water-based Condensation Particle Counter, CPC, TSI mod. 3787), and a commercial Aerodynamic Particle Sizer (APS, TSI). Particles from 14 nm to 750 nm of mobility diameter were sized and counted by the SMPS; particles from 0.5 to 20 μm of aerodynamic diameter were sized and counted by the APS (the procedure to fit the two PNSDs is described in the Sect.3.2). SMPS data were corrected for penetration errors through the sampling line, penetration efficiency due to diffusion losses (calculated according to Hinds (1999)) being higher than 98% for particles bigger than 14 nm. An impactor (nozzle of 0.457 μm) was used to remove larger particles.

3 Data analysis

Data measured by all the instruments were merged in a single dataset of 5 minute resolution. Dataset consisted of 3211 records (1764 in fall, and 1447 in winter). The statistical analysis was done on a subset of these data with no empty field (2551 records, covering 40 days of measurements). These data were then cleaned, and a final dataset of 1487 records (550 in fall, and 937 in winter) was ultimately included in the statistical analysis. The longer dataset was, however, used in the analysis to evaluate single cases (e.g., the case-study).

3.1 Inference of the optical Black Carbon mass concentration

The wavelength (λ) dependent BC absorption coefficient ($\sigma_{aBC}(\lambda)$), and equivalent BC mass concentration, were calculated using the AAE_{BC} attribution method. The measured absorption coefficient at 660 nm ($\sigma_a(660)$) was used to derive $\sigma_{aBC}(530)$, and then the BC mass concentration, assuming: (i) a known value of AAE_{BC} at 530-660 nm (see below), and (ii) BC Mass Absorption Efficiency at 530 nm to be 10 $\mathrm{m}^2\ \mathrm{g}^{-1}$ (as indicated by PSAP manufacturer). In literature, AAE_{BC}=1 is a commonly used value for externally mixed BC; internally mixed BC is commonly assumed to have the same AAE_{BC}=1. In fact, AAE_{BC} for externally mixed BC has been predicted to be 1 for particles with diameter $<$ 50 mm (e.g., Bergstrom et al., 2002; Moosmüller et al., 2011), but can range from 0.8 to 1.1 for particle diameters of 50-200 nm (Gyawali et al., 2009). For ambient particles, which can be internally or externally mixed, AAE_{BC} for visible wavelengths has often been observed to be larger than 1 (Lack and Langridge, 2013; Shinozuka et al, 2009, and references therein). Theoretical calculations have shown that the AAE_{BC} for internally mixed BC can vary from 0.55 (e.g., Bahadur et al., 2012) to an upper limit of $\sim$ 1.7 (e.g., Lack et al., 2008) depending on particle size, coating, core, wavelengths. Based on these works, we decided to use AAE_{BC}=1.1. The uncertainty was set to $\frac{\delta(AAE_{BC})}{AAE_{BC}}$=0.22 (Lack and Langridge, 2013). BC uncertainty ($\delta(BC)$)

was derived propagating this $\delta(AAE_{BC})$ together with the uncertainty of PSAP-derived σ_a (see Sect.2.2).

We discarded data possibly affected by desert dust (43 records over 5 days of measurements) to ensure that the equivalent BC mass concentration is not affected from contamination by desert dust. Dust-free aerosol conditions were identified based on the analysis of aerosol spectral optical properties, increasingly applied to gather information on aerosol type (e.g., Bergstrom et al., 2007; Clarke et al., 2007; Yang et al., 2009; Russell et al., 2010; Gyawali et al., 2012; Lee et al., 2012; Costabile et al., 2013) . We followed the methodology proposed by Costabile et al. (2013)(further discussed in Sect.5.2). Accordingly, the aerosol dominated by dust shows this distinctive combination of scattering, and absorption Ångström Exponents (SAE, AAE), and Single Scattering Albedo (SSA) spectral variation (dSSA): SSA_{530} >0.85, $SAE_{467-660}$ <0.5 , $AAE_{467-660}$ ∼2, $dSSA_{660-467}$=0.05-0.3. Data points of the time series fulfilling all these conditions together were excluded from the analysis.

3.2 Fitting procedure for the particle number size distribution

Data of particle number size distributions (PNSDs) were measured by two different instruments (SMPS and APS, Sect.2). These data were merged to obtain one PNSD based on particle electrical mobility diameters (d_m) ranging from 14 nm to 14 μm. PNSDs measured by APS are based on aerodynamic diameters (d_a); these data were converted to PNSDs based on d_m according to Eq.1 (Khlystov et al., 2004; Seinfeld and Pandis, 2006):

$$d_m = \chi \frac{C_c(d_m)}{C_c(d_a)} \frac{d_a}{(\frac{\rho_p}{\rho_0 \chi})^{1/2}} \quad (1)$$

where χ is the shape factor, $C_c(d_m)$ and $C_c(d_a)$ are the slip correction factors based on d_m and d_a respectively, ρ_p is the particle density, and ρ_0 is the unit density (1 g·cm^{-3}). In applying Eq.1 to convert APS data, we assumed: particle diameter (d_p) = d_m; $C_c(d_m)$ = 1 and $C_c(d_a)$ = 1 (continuum regime); χ = 1 (spherical particles); ρ_p continuously varying from 1.6 to 2 g·cm^{-3}.

Particle Number Size Distributions, $n_N(log_{10}d_m) = \frac{dN}{dlog_{10}(d_m)}$, measured by SMPS and APS ($PNSD_{SMPS}$, $PNSD_{APS}$) overlap for d_m ranging from 460 nm to 593 nm. In this size range, $PNSD_{SMPS}$ and $PNSD_{APS}$ were replaced by $PNSD_{fitted}$. $PNSD_{fitted}$ was assumed to vary according to a power-law function (Junge size distribution) (Khlystov et al., 2004; Seinfeld and Pandis, 2006) (Eq.2):

$$n_N(log_{10}d_m) = \frac{c}{d_m^{\alpha}}, \quad (2)$$

The coefficients c and α were calculated by an iterative procedure: (i) c was randomly initialized from 0 to 1000; (ii) α was calculated by Eq.2 constraining values from 2 to 5, as typically found for

atmospheric aerosols (Seinfeld and Pandis, 2006). $PNSD_{fitted}$ replaced $PNSD_{APS}$ and $PNSD_{SMPS}$ when their relative difference (d_r, Eq.4):

$$d_r = \frac{|PNSD_{SMPS} - PNSD_{APS}|}{max[PNSD_{SMPS}, PNSD_{APS}]} \quad (3)$$

was larger than 0.1 cm^{-3}. This procedure was considered acceptable if: (i) the minimum mean squared error between $PNSD_{fitted}$ and $PNSD_{APS}$ was less than 1%; (ii) correlation coefficients between $PNSD_{fitted}$ and $PNSD_{SMPS}$, and between $PNSD_{fitted}$ and $PNSD_{APS}$ were larger than 0.8. A number of 98 records did not verify these conditions, and were checked by visual inspection: 94 of them were discarded, and 4 accepted. The final dataset contained PNSD data based on d_m from 14.1 to 429.4 nm measured by the SMPS, from 446.1 to 699 nm generated by the fitting procedure, and from 0.7 to 14 μm measured by the APS .

4 Results and discussion

In this section, we first identify a "brown" aerosol (AAE from 2 to 6) by relating AAE to key aerosol populations extracted through a combined statistical analysis of PNSD, and organic aerosol mass spectra. We then characterise physico-chemical properties of the observed "brown" aerosol as regards number and mass size distribution (and relevant modes), and major PM_1 chemical components (BC, organics, nitrate, ammonium, and sulfate), relevant mass fractions, and ratios. A case-study is finally illustrated.

4.1 "Brown" aerosol: identification and features

Key aerosol types were identified through a statistical approach. PNSD principal components (PCs) were identified by Principal Component Analysis (PCA). PCA was calculated following the findings of a previous long-term study over multiple sites (8 concurrent stations) by Costabile et al. (2009). Four principal components (PC1-PC4) were extracted, explaining 90% of the variance. We interpreted these PCs based on: (i) their statistical properties, i.e. "scores" and "loadings" (loadings indicate correlations between PNSDs and PCs, i.e. the "mode" of the PNSD associated to the PC); (ii) Pearson's correlation coefficients (r) shown in Table 1, between PCs, AAE, and PM_1 mass fractions of BC, organics, nitrate, sulfate, and ammonium (f_{BC}, f_{OA}, f_{NO3}, f_{SO4}, f_{NH4}). The median diameter of the particle surface size distribution ($d_{med(S)}$) in Table 1 is intended to add information on optically relevant aerosol sizes. The OA to BC ratio (OA-to-BC) in Table 1 is intended to indicate both combustion characteristics (higher for biofuels than for fossil fuel combustion), and aerosol ageing (lower for fresh aerosols) (Saleh et al., 2014; Bond et al., 2013). Correlations to f_{43} and f_{44} (defined as the ratio of the AMS signal at m/z 43 and m/z 44, respectively, to the total organics AMS signal) in Table 1 are intended to add information on the oxidised OA. The higher the f_{44}, the more

oxidised the OA; the higher the f_{44}/f_{43} ratio, the lower the volatility of this oxidised OA (Ng et al., 2010, 2011; Moise et al., 2015).

Statistical properties used to interpret PC are "scores" and "loadings". PCs retained in the analysis were arranged in decreasing order of variance explained ($\varkappa_k$, called eigenvalue of PC_k), PC1 being the component explaining the largest $\varkappa_k$. The k^{th} eigenvector is composed of scalar coefficients describing the new PC_k as a linear combination of the original variables (the original variables are the time series of dN/dlog(d_p)). Coefficient of PC_k represent the relative weight (in terms of correlation) of dN/dlog(d_p) variables in PC_k. Factor loadings of PC_k represent these coefficients scaled by the $\varkappa_k$ explained by PC_k. Loadings of PC_k thus represent the relative weight of dN/dlog(d_p) variables in PC_k re-scaled by the $\varkappa_k$ explained by PC_k. Factor scores of PC_k are the transformed variables corresponding to a particular data point in the time series of the dN/dlog(d_p) variables. Factor scores thus represent the PC_k values corresponding to each particular data point of the dN/dlog(d_p) time series.

Weekly diurnal cycles, and loadings of PC1-4 are illustrated in supplemantary material. PC1, PC2, and PC4 are BC primary aerosol (all correlated to BC and f_{BC}). PC1 and PC4 are both sourced by traffic emissions, diurnal cycles peaking at rush hours and week-days. PC1 is a fine mode aerosol component (the PNSD mode peaking from 100 to 200 nm), PC4 an ultrafine aerosol component (PNSD peaking from 20 to 40 nm). PC2 is an ultrafine BC aerosol component, as PC4. Unlike PC4, however, PC2 higher scores are at night-time, and there is no weekly cycle and no peak at "rush hours": PC2 is probably sourced by heating emissions.

The remaining PC3 (more than 10% of the variance) relates to a secondary aerosol. It is the only PC inversely correlated to f_{BC}, and directly correlated to f_{OA}, f_{44}, OA-to-BC, and $d_{med(S)}$, with higher scores at daytime and during week days, the PNSD peaking in the accumulation mode (supplementary material). To enhance the interpretation of the aerosol type represented by this PC, Fig. 1 shows its factor loadings (brown line) in comparison to those of a PC from a previous study (Costabile et al., 2009), which has very similar statistical properties. This PC was found to represent the droplet mode aerosol. The droplet mode is a submode of the accumulation mode, resulting from the activation of condensation mode particles to form cloud/fog drops, followed by aqueous-phase chemistry, and droplet evaporation (John, 1990; Meng and Seinfield , 1994; Seinfeld and Pandis, 2006; Ervens et al., 2011). To our knowledge, the work by Costabile et al. (2009) is the only work in literature showing a similar PC to compare with: authors based its interpretation on five PCAs calculated on a two year dataset over eight concurrent measurement sites, correlated to meteorological and air quality data (green, blue, red, and black lines in Fig.1 indicate the droplet mode PC identified by these five PCAs, calculated by varying the dataset time lenght and number of measurement sites). The broad similarities between this PC and PC3 allow to deduce with a reasonable statistical accuracy that PC3 does represent the droplet mode aerosol, as well. This comparison ultimately demostrates that the "brown" aerosol is secondary in origin (the droplet mode is secondary in origin,

because formed through secondary processes in the atmosphere (John, 1990; Meng and Seinfield , 1994)), and gives insights into its likely formation process. This conclusion is reinforced by the correlation with f_{44} (Tab. 1).

In Table 1, it is indicated a robust statistical relation linking AAE, this "droplet" mode component (PC3), and OA-to-BC, together with f_{OA}, $d_{med(S)}$, f_{44} and f_{43}. Figure 2 shows this relation. When the droplet mode PC scores positive (PC scores >0 indicate that this aerosol type forms), the AAE is greater than 2.5. Both AAE and droplet mode increase with increasing OA-to-BC, and f_{44}, both indicators of OA aged in the atmosphere (Ng et al., 2010; Bond et al., 2013). Data, therefore, identify a "brown" aerosol type, i.e. an aerosol showing AAE from 2.5 to 6, having high "droplet" mode PC scores. The dependence of this "brown" aerosol on PM_1 major costituents, and relevant ratios, is illustrated in Fig. 3 and Fig. 4, where the brown aerosol formation is indicated by the combined increase of AAE (y-axis) and droplet mode PC score (marker color). This "brown" aerosol formation depends on the organic mass fraction (f_{OA}, Fig.3a), and is inversely correlated to the mass fractions of BC (f_{BC}, Fig.3b), and sulfate (f_{SO4}, Fig.3c). The dependence on the nitrate mass fraction (f_{NO_3}, Fig.3d) is not obvious, as high AAE values and droplet mode scores are observed for both f_{NO_3} <0.05 and f_{NO_3} $\simeq$0.25.

The relation between this "brown" aerosol and the BC-to-OA ratio (or its inverse OA-to-BC ratio = f_{OA}/f_{BC}) is shown in Fig. 4. Uncertainties of AAE, and BC-to-OA in Fig.4 were calculated propagating uncertainties of PSAP-derived σ_a (Sect.2.2), BC derived by the AAE_{BC} attribution method (Sect.3.1), and AMS-derived OA (Sect.2.3). The area showing the brown aerosol (AAE from 2.5 to 6.6, positive droplet mode PC scores) has high OA-to-BC ratios (note correlation r = 0.78 between AAE and OA-to-BC ratio, Table 1). The inverse dependence between this "brown" aerosol formation and the BC-to-OA ratio confirms results of the statistical analysis (correlations with f_{44} and f_{43}) indicating that the brown aerosol is an aged OA. Indeed, it is typical that BC contribution declines, and OA contribution increases, as the smoke aerosol ages in the atmosphere. Relative proportions of BC and OA in the AAE vs BC-to-OA relation are indicated in the supplementary material. It is shown that the increase in AAE with decreasing the BC-to-OA ratio is not simply due to the decreased contribution of BC. The AAE of the aerosol is indeed dictated by the relative contribution of the OA and BC components. There is a small trend of the lowest AAE values toward 1.5, rather than 1. We explain this if we first consider that the variability from 1 to 1.5 of AAE is within the uncertainty of the instrumentation. And second, if we consider that these low AAE values are at OA values larger than zero (Suppl. material), similarly to previous results (Lack et al., 2008). The AAE larger than 1 can hence be due to any spectrally light absorbing material that the AMS could not detect (refractory material, or material in particles smaller than 100 nm and larger than 1 μm).

Taken together, findings finally suggest that the "brown" aerosol type observed in the Po Valley, is secondary in origin and contains aged OA in "droplet" mode particles.

4.2 A case study

We present here a case study to visualize main aerosol features of the "brown" aerosol observed. The values of this case study were indicated in Fig. 4 by "*": they represent the highest values of AAE, and droplet mode PC scores observed, and thus a case of brown aerosol formation. Figure 5 (panels a, b, c) compares mean values of volume and mass size distributions measured over the whole field experiment with relevant values measured during this case study (first of February, 2013 from 17:30 to 19:00). Relative humidity (RH) was high (97.5$\pm$0.4%, against a mean value for the winter campaign of 82 $\pm$ 14 %, and a maximum of 98 %), temperature averaged 2.8 $\pm$ 0.0 $^\circ$ C (campaign mean value=3.5 $\pm$ 2.8 $^\circ$ C). Aerosol vertical profiles from a LD40 ceilometer (Fig. 5d) indicate a foggy day, except for the middle part of the day (from 11:00 to 15:00) when the fog layer is shown to dissipate. The day started with low concentrations of sub-micrometer aerosol particles (Fig. 5e). Coarse mode aerosol particles increased in the early hours of the day, and then decreased, followed by the increase of droplet mode aerosol particles (as indicated by the area in Fig. 5e corresponding to diameters ranging from 500 to 800 nm, and PC3 scores - not shown here). We interpret this as formation of fog drops, followed by droplet evaporation, and aerosol droplet mode formation, a plausible mechanism for formation of this aerosol type (John, 1990; Meng and Seinfield , 1994; Seinfeld and Pandis, 2006). AAE (Fig. 5f) was significantly higher than its mean value (up to more than 6 - unfortunately no data is available before 15:00). Relevant volume size distribution (Fig. 5a) is centered on the droplet mode (d_m from 450 to 700 nm), the peak being more than four times as high as that of the mean value. Mass size distributions of the main constituents of nr-PM_1 (NO_3, organics, and NH_4) are centered around 700 nm of the vacuum aerodynamic diameter (d_{va}). Note that d_{va} = 700 nm corresponds to d_m = 468 nm for spherical particles with $\rho_p = 1.5g \cdot cm^{-3}$ in the continuum regime, as d_m and d_{va} are linked by Eq.4 (Seinfeld and Pandis, 2006) :

$$d_{va} = d_m \frac{\rho_p}{\rho_0}. \quad (4)$$

In addition, the organic aerosol mass below d_{va} = 300 nm was significantly lower than that of the droplet mode, especially when compared to the average field results (Fig. 5c). Relevant absorption and scattering coefficients (not shown here) ranged from 5 to 10 Mm^{-1}, and from 300 to 400 Mm^{-1}, respectively. As shown by this case study, a general feature of the whole field campaign was that the brown aerosol formed in the early afternoon.

5 Discussion in comparison with previous works

In this section, we discuss findings to explore consistency with literature, and put results in a broader perspective.

5.1 "Brown" aerosol in the ambient atmosphere

In Figure 6, relations illustrated in Fig.3 and Fig. 4 between AAE, f_{OA}, and f_{OA}/f_{BC} = OA-to-BC, are compared to literature. Our results (obtained in urban ambient air) are compared to previous findings obtained under "diluted" urban conditions (airborne, and AERONET columnar observations) (Shinozuka et al, 2009; Russell et al., 2010), or in combustion chambers experiments (Saleh et al., 2014; Lu et al., 2015).

Figure 6a shows the relation between AAE (y axis), f_{OA} (x axis), SSA (at 530 nm, marker color), and $d_{med(S)}$ (marker size). The Pearson's correlation coefficient (r) is 0.56. Fig. 6a is intended to compare to Russell et al. (2010)'s results, indicated by the black line, and Shinozuka et al (2009)'s results, indicated by grey lines. Note that grey lines by Shinozuka et al (2009) refer to the SSA bins of 0.90-0.92, 0.96-0.98 and 0.98-1.00. There are broad similarities between the three results. As in Russell et al. (2010)'s and Shinozuka et al (2009)'s work, our data make evident that increasing f_{OA} values are accompanied by increasing AAE values, when dust is absent. However, there are conditions when AAE increases irrespective of f_{OA}. In contrast, when f_{OA} is normalised to f_{BC} (f_{OA}/f_{BC} = OA-to-BC ratio), there is a strong correlation with AAE (r = 0.78, Fig. 6b). The increasing OA-to-BC ratio is accompanied by a uniform increase of AAE. As well, there is a weak increase of SSA (r = 0.56), and $d_{med(S)}$ (r = 0.49). As in Shinozuka et al (2009)'s results for SSA bins 0.98-1.00, it is shown that values of AAE>3.5 are at SSA $>$ 0.98 (Fig. 6a). Note values measured during the case study (Fig. 5) indicated by "*". All of them are at these high AAEs. This comparison ultimately shows (i) consistency of "brown" aerosol properties observed from airborne/AERONET, and measured in situ at the ground; (ii) OA-to-BC ratio to be a better indicator than f_{OA} of "brown" aerosol and its large AAE values.

Saleh et al. (2014) used the inverse of OA-to-BC to parametrize the AAE of biomass burning emissions in a combustion chamber experiment. To compare to Saleh et al. (2014)'s and Lu et al. (2015)'s work, panel c of Fig.6 shows AAE versus BC-to-OA (the inverse in log scale of the x axis in Fig. 6b). Black and grey lines in Fig.6c indicate Saleh et al. (2014)'s and Lu et al. (2015)'s least-square-fit, respectively. There are similar patterns. Both Saleh et al. (2014) and Lu et al. (2015) concluded that this dependence of AAE on the BC-to-OA ratio can be observed solely for biomass burning OA, and not for fossil fuel OA. Note that we compare, in Fig.6c, different AAE values. In our work, AAE values are due to the whole dust-free aerosol, thus depending on both BC and OA ($AAE_{BC,OA}$). AAE values of Saleh et al. (2014) and Lu et al. (2015) (AAE_{OA}) come from the wavelength-dependence of OA alone (w_{OA}), excluding contributions from BC (AAE_{OA} values are calculated from w_{OA} based on the relation AAE=w+1, valid for small particles in the visible range). The comparison in Fig.6c is thus intended to compare patterns only, not absolute values. In the Supplementary material, AAE_{BC} is plotted together with $AAE_{BC,OA}$, in the AAE vs BC-to-OA plot. This figure is intended to indicate wavelenght dependence of OA absorption, and suggest

possible AAE_{OA} patterns, increasing with decreasing BC-to-OA, similarly to what observed by Saleh et al. (2014) and Lu et al. (2015).

This comparison strenghtens our findings indicating that the "brown" aerosol (i) represents an aerosol aged in the atmosphere, and (ii) is not a freshly emitted aerosol, as it is not observed in a combustion chamber experiment. If Saleh et al. (2014)'s results are confirmed, this comparison suggests that this brown aerosol derives from the processing of biomass burning OA. It is worth noting that the AAE of this secondary "brown" aerosol would probably be higher than that of the fresh biomass burning OA it likely derives from. Lu et al. (2015)'s experiments similarly suggested that atmospheric processing should not decrease biomass burning OA absorptive properties.

5.2 Spectral optical properties of the "brown" aerosol

Cluster analysis of aerosol spectral optical properties is becoming more and more used to infer information on aerosol type from optical data (e.g., Bergstrom et al., 2007; Clarke et al., 2007; Yang et al., 2009; Russell et al., 2010; Gyawali et al., 2012; Lee et al., 2012; costabile2013). This analysis holds promise for future aerosol classification from remote optical measurements (e.g., AERONET, satellite). Costabile et al. (2013) assessed spectral optical properties of key aerosol populations through Mie theory: soot, biomass burning, two types of organics, dust and marine particles were simulated through a sectional approach where each of these aerosol types was given a monomodal PNSD and a set of three refractive indices (RIs) in the visible range. Relevant Ångström Exponents of extinction, scattering, and absorption (EAE, SAE, AAE), SSA and its spectral variation (dSSA) were calculated. It was proved that these aerosol types separately cluster within a "paradigm" where SAE is on the y-axis, dSSA times AAE is on the x-axis, and SSA is on the z-axis (Fig. 7).

In this section, we show that experimental data of the "brown" aerosol do cluster in this paradigm, as well (Fig. 7), and that the cluster of "brown" aerosol data is separated from all other simulated aerosol types, except that named "large organics". Data of "large organics" and "brown" aerosol do overlap, indicating that they may represent the same aerosol type. In fact, microphysical properties of the aerosol type named "large organics" were simulated to be same as those of the droplet mode aerosol (i.e., PNSD peaking in the "large" accumulation mode, 300-800 nm size range). Spectral optical properties of this "large organics" aerosol type were simulated by RIs of spectrally absorbing organic material in the visible region: these RIs, given the broad similarities in Fig.7, can be assumed to be those of the "brown" aerosol.

This comparison ultimately allows to infer spectral otpical properties of "brown" aerosol (Table.2), definitely not a purely scattering component. It is worth noting that the value of k_{530} assumed for the "brown" aerosol is consistent with literature k_{530} values recently reviewed by Lu et al. (2015) for the bulk OA obtained from chemically aged primary aerosol. Supplementary material shows the variability of relevant spectral optical properties with varying mass fractions of PM_1 major components.

5.3 A SOA type "brown" aerosol

Findings indicate a relation linking the "brown" aerosol to the aged OA. AMS measurements enable to map OA ageing level by combining f_{43} and f_{44} (Sect. 4.1, and Table 1), representing intensities of the two oxygen-containing ions domining the OA spectra (see review by Moise et al., 2015). f_{44} has been found to originate from the dissociation in the AMS of oxidised organic molecules (the CO_2^+ fragment from carboxylic acid groups). f_{43} has been related to non-acid oxidised species (the $C_2H_3O^+$ fragment from aldehydes and ketones), in addition to saturated hydrocarbons (the $C_3H_7^+$ fragment). Figure 8 shows f_{44} plotted against f_{43}, and their relation with the brown aerosol (AAE is data color, the droplet mode PC score is data size). This figure is intended to reproduce the "triangle plot" proposed by Ng et al. (2011, 2010), which encompasses the majority of OA values measured in ambient samples. It is showed that the "brown" aerosol (the largest yellow-to-red markers) lies in the oxidised OA region, where most of the semi volatile oxidised OA measurements taken at the ground lie (Ng et al., 2010; Crippa et al., 2014). The composition found for this "brown" aerosol (high OA, nitrates being a likely component), its formation process (involving aqueous phase reactions), and AAEs values, are all coherent with previous studies, which showed increased light absorption towards UV for SOA particles (Jacobson, 1999; Lee et al., 2013; Song et al., 2013; Zhang et al., 2013; Powelson et al., 2014; Lin et al., 2014; Laskin et al., 2015), and sources, composition, and AAE of light-absorbing soluble organic aerosol in urban areas (Zhang et al., 2013, 2011) .

This comparison reinforces our hypothesis that the "brown" aerosol is an aged OA.

6 Summary and conclusions

We characterized the nondust aerosol having the strongest spectral dependance of light absorption (as indicated by the Absorption Ångström Exponent, AAE) at visible wavelengths in the urban ambient atmosphere of the Po Valley (Bologna). We defined "brown" this bulk aerosol with brown color (it does not necessarily equate to brown carbon). In situ ground ambient measurements of chemical (HR-ToF-AMS), optical (3-λ nephelometer and PSAP), and micro-physical (SMPS and APS) aerosol properties were taken, together with ancillary observations.

Findings prove that the observed "brown" aerosol is a secondary aerosol dominated by accumulation mode particles containing organic aerosol (OA).

Conditions when "brown" aerosol dominates the bulk dust-free aerosol were first identified based on AAE values. "Brown" aerosol sources in the urban atmosphere were then investigated by relating these AAE to key aerosol populations statistically identified. Physico-chemical properties of this aerosol were characterised: number and mass size distribution, major PM_1 chemical components (BC, organics, nitrate, ammonium, and sulfate), their mass fractions, and relevant ratios (including the BC-to-OA ratio). A case-study was illustrated. Overall, the "brown" aerosol has AAE values from 2.5 to 6, is secondary in origin, formed by the larger accumulation mode particles referred to

in literature as droplet mode particles, and contains large concentrations of organic aerosol (OA), its OA-to-BC ratio being higher. Nitrate is an additional likely component.

To our knowledge, no previous work has considered these issues in the ambient atmosphere. This is the first experimental evidence that extends observations by Saleh et al. (2014) to ambient conditions, and provides a micro-physical characterization of this "brown" aerosol.

Consistency of findings with literature was then explored. We compared our results with previous findings obtained for "diluted" urban aerosols (airborne and AERONET observations), and freshly emitted aerosols (combustion chamber experiments). We found a dependence of AAE on OA similar to what found for airborne and AERONET data, and a dependence of AAE on the BC-to-OA ratio similar to what found for freshly emitted aerosols. Our study adds to these previous studies that: (i) AAE depends on the OA-to-BC ratio more than on OA, and (ii) the link between AAE and the OA-to-BC (already observed for the freshly emitted primary aerosol from biomass burning) is observed in the ambient atmosphere, as well, where it can be used to identify the "brown" aerosol. Finally, the comparison with a simulation work allowed to obtain the following optical signature in the visible region for the "brown" aerosol: AAE of 2.5-6.6, SAE of 0.5-2, SSA of 0.9-1, and average refractive index at 467 nm of 1.460-0.012i.

Findings will have important atmospheric implications for modeling studies, and remote sensing observations. The link between AAE and the OA-to-BC ratio can be a strong tool to parametrize the "brown" aerosol in the atmosphere, as well as to investigate brown OA and Brown Carbon. It is worth noting that this link can be used to extrapolate preliminary chemical information from optical ones, as optical techniques are increasingly used to characterise aerosol properties.

Acknowledgements. This work was realized in the framework of the Supersito Project. The work was partly accomplished in the framework of the DIAPASON ("Desert-dust Impact on Air quality through model-Predictions and Advanced Sensors ObservatioNs") project, funded by the European Commission (LIFE+ 2010 ENV/IT/391).

References

Andreae, M. O. and Gelencsér, A.: Black carbon or brown carbon? The nature of light-absorbing carbonaceous aerosols, Atmos. Chem. Phys., 6, 3131-3148, doi:10.5194/acp-6-3131-2006, 2006.

Arola, A., Schuster, G., Myhre, G., Kazadzis, S., Dey, S., and Tripathi, S. N.: Inferring absorbing organic carbon content from AERONET data, Atmos. Chem. Phys., 11(1), 215-225, 2011.

Backman, J., Virkkula, A., Vakkari, V., Beukes, J. P., Van Zyl, P. G., Josipovic, M., Piketh, S., Tiitta, P., Chiloane, K., Petäjä, T., Kulmala, M., and Laakso, L.: Differences in aerosol absorption Ångström exponents between correction algorithms for a particle soot absorption photometer measured on the South African Highveld, Atmos. Meas. Tech., 7, 4285-4298, doi:10.5194/amt-7-4285-2014, 2014.

Bahadur, E., Praveen, P. S., Xu, Y., and Ramanathan, V.: Solar absorption by elemental and brown carbon determined from spectral observations, P. Natl. A. Sci., 109, 17366-17371, 2012.

Bellouin, N.. Aerosols: The colour of smoke, Nat. Geosci., 7(9), 619-620, 2014.

Bergstrom, R. W., Russell, P. B., and Hignett, P.: Wavelength Dependence of the Absorption of Black Carbon Particles: Predictions and Results from the TARFOX Ex Atmos. Chem. Phys., 13, 10535-10543, 2013.

Bond, T. C., Anderson, T. L., and Campbell, D.: Calibration and intercomparison of filter-based measurements of visible light absorption by aerosols, Aerosol Sci. Tech., 30, 582-600, 1999.

Bond, T.C., Doherty, S.J., Fahey, D.W., Forster, P. M., Berntsen,T., DeAngelo, B.J., Flanner, M.G., Ghan,S., Kärcher, B., Koch, D., Kinne, S., Kondo, Y., Quinn, P.K., Sarofim, M.C., Schultz, M.G., Schulz, M., Venkataraman, C., Zhang, H., Zhang, S., Bellouin, N., Guttikunda, S. K., Hopke, P. K., Jacobson, M. Z., Kaiser, J. W., Klimont, Z., Lohmann, U., Schwarz, J. P., Shindell, D., Storelvmo, T., Warren, S.G., Zender, C.S.: Bounding the role of black carbon in the climate system: A scientific assessment, J. Geophys. Res. Atmos., 118, 5380-5552, doi:10.1002/jgrd.50171, 2013.

Cappa, C. D., Lack, D. A., Burkholder, J. B., Ravishankara, A. R.: Bias in filter-based aerosol light absorption measurements due to organic aerosol loading: Evidence from laboratory measurements. Aerosol Science and Technology, 42(12), 1022-1032, 2008.

Costabile, F., Birmili, W., Klose, S., Tuch, T., Wehner, B., Wiedensohler, A., Franck, U., König, K., and Sonntag, A.: Spatio-temporal variability and principal components of the particle number size distribution in an urban atmosphere, Atmos. Chem. Phys., 9, 3163-3195, doi:10.5194/acp-9-3163-2009, 2009.

Costabile, F., Barnaba, F., Angelini, F., and Gobbi, G. P.: Identification of key aerosol populations through their size and composition resolved spectral scattering and absorption, Atmos. Chem. Phys., 13, 2455-2470, doi:10.5194/acp-13-2455-2013, 2013.

Costabile, F., Angelini, F., Barnaba, F., Gobbi, G. P.: Partitioning of Black Carbon between ultrafine and fine particle modes in an urban airport vs. urban background environment, Atmos. Environ., 102, 136-144, 2015.

Crippa, M., Canonaco, F., Lanz, V. A., Äijälä, M., Allan, J. D., Carbone, S., Capes, G., Ceburnis, D., Dall'Osto, M., Day, D. A., DeCarlo, P. F., Ehn, M., Eriksson, A., Freney, E., Hildebrandt Ruiz, L., Hillamo, R., Jimenez, J. L., Junninen, H., Kiendler-Scharr, A., Kortelainen, A.-M., Kulmala, M., Laaksonen, A., Mensah, A. A., Mohr, C., Nemitz, E., O'Dowd, C., Ovadnevaite, J., Pandis, S. N., Petäjä, T., Poulain, L., Saarikoski, S., Sellegri, K., Swietlicki, E., Tiitta, P., Worsnop, D. R., Baltensperger, U., and Prévôt,, A. S. H.: Organic aerosol components derived from 25 AMS data sets across Europe using a consistent ME-2 based source apportionment approach, Atmos. Chem. Phys., 14, 6159-6176, doi:10.5194/acp-14-6159-2014, 2014.

DeCarlo, P. F., Kimmel, J. R., Trimborn, A., Northway, M. J., Jayne, J. T., Aiken, A. C., Gonin, M., Fuhrer, K., Horvath, T., Docherty, K. S., Worsnop, D. R., and Jimenez, J. L.: Field-deployable, high-resolution, time-of-flight aerosol mass spectrometer, Anal. Chem., 78, 8281-8289, 2006.

Ervens, B., Turpin, B. J., and Weber, R. J.: Secondary organic aerosol formation in cloud droplets and aqueous particles (aqSOA): a review of laboratory, field and model studies, Atmos. Chem. Phys., 11, 11069-11102, doi:10.5194/acp-11-11069-2011, 2011.

Gyawali, M., Arnott, W. P., Lewis, K., and Moosmüller, H.: In situ aerosol optics in Reno, NV, USA during and after the summer 2008 California wildfires and the influence of absorbing and non-absorbing organic coatings on spectral light absorption, Atmos. Chem. Phys., 9, 8007-8015, doi:10.5194/acp-9-8007-2009, 2009.

Hinds W.C., Aerosol Technology, 2nd, Edition., Wiley, New York, 1999.

Khlystov, A., Stanier,C., Pandis, S. N.: An Algorithm for Combining Electrical Mobility and Aerodynamic Size Distributions Data when Measuring Ambient Aerosol, Special Issue of Aerosol Science and Technology on Findings from the Fine Particulate Matter Supersites Program., Aerosol Sci. Tech., 38, S1, 229-238, 2004.

Lack, D.A., Cappa, C.D., Covert, D.S., Baynard, T., Massoli, P., Sierau, B., Bates, T.S., Quinn, P.K., Lovejoy, E.R. and Ravishankara, A.R.: Bias in filter-based aerosol light absorption measurements due to organic aerosol loading: Evidence from ambient measurements. Aerosol Science and Technology, 42(12), pp.1033-1041, 2008.

Lack, D. A. and Langridge, J. M.: On the attribution of black and brown carbon light absorption using the Ångström exponent, Atmos. Chem. Phys., 13, 10535-10543, doi:10.5194/acp-13-10535-2013, 2013.

Laskin, A., Laskin, J., and Nizkorodov, S. A.: Chemistry of Atmospheric Brown Carbon, Chem. Rev., doi: 10.1021/cr5006167, 2015.

Lee, A.K.Y., Zhao, R., Li, R., Liggio, J., Li, S.-M., Abbatt, J.P.D.: Formation of light absorbing organo-nitrogen species from evaporation of droplets containing glyoxal and ammonium sulfate, Environ. Sci. Technol., 47 (22), 12819-12826, doi:10.1021/es402687w, 2013.

Lin, Y.-H., Budisulistiorini, S.H., Chu, K., Siejack, R.A., Zhang, H., Riva, M., Zhang, Z., Gold, A., Kautzman, K.E., Surratt, J.D.: Light-absorbing oligomer formation in secondary organic aerosol from reactive uptake of isoprene epoxydiols, Environ. Sci. Technol., 48 (20), 12012-12021, doi: 10.1021/es503142b, 2014.

Lu, Z., Streets, D.G., Winijkul, E., Yan, F., Chen, Y., Bond, T.C., Feng, Y., Dubey, M.K., Liu, S., Pinto, J.P., Carmichael, G.R.: Light absorption properties and radiative effects of primary organic aerosol emissions, Environ. Sci. Technol., 49 (8), 4868-4877, doi: 10.1021/acs.est.5b00211, 2015.

Jacobson, M. Z.: Isolating nitrated and aromatic aerosols and nitrated aromatic gases as sources of ultraviolet light absorption, J. Geophys. Res. - Atmos., 104(D3), 3527-3542, 1999.

Jimenez, J. L., Jayne, J.T., Shi, Q., Kolb, C.E., Worsnop, D.R., Yourshaw, I., Seinfeld, J.H., Flagan, R.C., Zhang, X., Smith, K.A. and Morris, J.W.: Ambient aerosol sampling using the Aerodyne Aerosol Mass Spectrometer, J. Geophys. Res. - Atmos., 108 (D7), 1984-2012, doi:10.1029/2001jd001213, 2003.

John, W., Wall, S. M., Ondo, J. L., and Winklmayr, W.: Modes in the size distributions of atmospheric inorganic aerosol, Atmos. Environ., 24A, 2349-2359, 1990.

Meng, Z. and Seinfield, J. H.: On the source of the submicrometer droplet mode of urban and regional aerosols, Aerosol Sci. Tech., 20, 253-265, 1994.

Middlebrook, A. M., Bahreini, R., Jimenez, J. L. and Canagaratna, M. R.: Evaluation of Composition-Dependent Collection Efficiencies for the Aerodyne Aerosol Mass Spectrometer using Field Data, Aerosol Sci. Tech., 46, 258-271, doi:10.1080/02786826.2011.620041, 2012.

Moise,T., Flores, J.M., Rudich, Y.: Optical Properties of Secondary Organic Aerosols and Their Changes by Chemical Processes, Chem. Rev., 115.10, 4400-4439, doi: 10.1021/cr5005259, 2015.

Moosmüller, H., Chakrabarty, R. K., Ehlers, K. M., and Arnott, W. P.: Absorption Ångström coefficient, brown carbon, and aerosols: basic concepts, bulk matter, and spherical particles, Atmos. Chem. Phys., 11, 1217-1225, doi:10.5194/acp-11-1217-2011, 2011.

Ng, N. L., Canagaratna, M. R., Zhang, Q., Jimenez, J. L., Tian, J., Ulbrich, I. M., Kroll, J. H., Docherty, K. S., Chhabra, P. S., Bahreini, R., Murphy, S. M., Seinfeld, J. H., Hildebrandt, L., Donahue, N. M., DeCarlo, P. F., Lanz, V. A., Prévôt, A. S. H., Dinar, E., Rudich, Y., and Worsnop, D. R.: Organic aerosol components observed in Northern Hemispheric datasets from Aerosol Mass Spectrometry, Atmos. Chem. Phys., 10, 4625-4641, doi:10.5194/acp-10-4625-2010, 2010.

Ng, N. L., Canagaratna, M. R., Jimenez, J. L., Chhabra, P. S., Seinfeld, J. H., and Worsnop, D. R.: Changes in organic aerosol composition with aging inferred from aerosol mass spectra, Atmos. Chem. Phys., 11(13), 6465-6474, 2011.

Pöschl, U.: Aerosol particle analysis: challenges and progress. Anal. Bioanal. chem., 375.1, 30-32, DOI 10.1007/s00216-002-1611-5, 2003.

Powelson, M.H., Espelien, B.M., Hawkins, L.N., Galloway, M.M., De Haan, D.O.: Brown carbon formation by aqueous-phase carbonyl compound reactions with amines and ammonium sulfate, Environ. Sci. Technol., 48 (2), 985-993, doi: 10.1021/es4038325, 2014.

Quinn, P. K., Bates, T. S., Coffman, D. J., and Covert, D. S.: Influence of Particle Size and Chemistry on the Cloud Nucleating Properties of Aerosols, Atmos. Chem. Phys. 8(4), 1029-1042, 2008.

Russell, P. B., Bergstrom, R. W., Shinozuka, Y., Clarke, A. D., DeCarlo, P. F., Jimenez, J. L., Livingston, J. M., Redemann, J., Dubovik, O., and Strawa, A.: Absorption Ångström Exponent in AERONET and related data as an indicator of aerosol composition, Atmos. Chem. Phys., 10, 1155-1169, doi:10.5194/acp-10-1155-2010, 2010.

Saleh, R., Hennigan, C. J., McMeeking, G. R., Chuang, W. K., Robinson, E. S., Coe, H., Donahue, N. M., and Robinson, A. L.: Absorptivity of brown carbon in fresh and photo-chemically aged biomass-burning emissions, Atmos. Chem. Phys., 13, 7683-7693, doi:10.5194/acp-13-7683-2013, 2013.

Saleh, R., Robinson, E. S., Tkacik, D. S., Ahern, A. T., Liu, S., Aiken, A. C., Sullivan, R. C., Presto, A. A., Dubey, M. K., Yokelson, R. J., Donahue, N. M., and Robinson, A. L.: Brownness of organics in aerosols from biomass burning linked to their black carbon content, Nat. Geosci., 7, 647-650, 2014.

Seinfeld, J. H. and Pandis, S. P.: Atmospheric Chemistry and Physics, 2nd edn., John Wiley, New York, USA, 1232 pp., 2006.

Shapiro, E. L., Szprengiel, J., Sareen, N., Jen, C. N., Giordano, M. R., and McNeill, V. F.: Light-absorbing secondary organic material formed by glyoxal in aqueous aerosol mimics, Atmos. Chem. Phys., 9, 2289-2300, doi:10.5194/acp-9-2289-2009, 2009.

Shinozuka, Y., Clarke, A. D., DeCarlo, P. F., Jimenez, J. L., Dunlea, E. J., Roberts, G. C., Tomlinson, J. M., Collins, D. R., Howell, S. G., Kapustin, V. N., McNaughton, C. S., and Zhou, J.: Aerosol optical properties

relevant to regional remote sensing of CCN activity and links to their organic mass fraction: airborne observations over Central Mexico and the US West Coast during MILAGRO/INTEX-B, Atmos. Chem. Phys., 9, 6727-6742, doi:10.5194/acp-9-6727-2009, 2009.

Song, C., Gyawali, M., Zaveri, R.A., Shilling, J.E., Arnott, W.P.: Light absorption by secondary organic aerosol from α-pinene: Effects of oxidants, seed aerosol acidity, and relative humidity, J. Geophys. Res., 118 (20), 11741-11749, doi: 10.1002/jgrd.50767, 2013.

Virkkula, A., Ahlquist, N. C., Covert, D. S., Arnott, W. P., Sheridan, P. J., Quinn, P. K., and Coffman, D. J.: Modification, calibration and a field test of an instrument for measuring light absorption by particles, Aerosol Sci. Tech., 39, 68–83, 2005.

Virkkula, A.: Correction of the calibration of the 3-wavelength Particle Soot Absorption Photometer (3λPSAP), Aerosol Sci. Tech., 44, 706–712, 2010.

Zhang, X., Lin, Y. H., Surratt, J. D., Zotter, P., Prévˆt, A. S., Weber, R. J.:. Light-absorbing soluble organic aerosol in Los Angeles and Atlanta: A contrast in secondary organic aerosol. Geophys. Res. Lett., 38(21), 2011.

Zhang, X., Y.-H. Lin, J. D. Surratt, and R. J. Weber: Sources, composition and absorption Ångström exponent of light-absorbing organic components in aerosol extracts from the Los Angeles Basin, Environ. Sci. Technol., 47(8), 3685-3693, 2013.

TABLES

Table 1. Pearson's correlation coefficients (r) between: Absorption Ångström Exponent (AAE); scores of principal components (PC1-PC4) of particle number size distributions obtained by Principal Component Analysis (PCA); mass fractions of Black Carbon (f_{BC}), organics (f_{OA}), nitrate (f_{NO3}), sulfate (f_{SO4}), and ammonium (f_{NH4}); median diameter of the particle surface size distribution ($d_{med(S)}$); BC mass concentration (BC); organic aerosol (OA) to BC ratio (OA-to-BC); ratio of the AMS signal at m/z 44 and m/z 43 to the total organics AMS signal (f_{44} and f_{43}). Note that PC3 is the "droplet" mode PC.

r	AAE	$d_{med(S)}$	BC	f_{BC}	f_{OA}	OAtoBC	f_{NO3}	f_{SO4}	f_{NH4}	f_{44}	f_{43}
AAE		0.48	-0.26	-0.37	0.56	0.78	-0.31	-0.44	-0.41	0.45	0.45
PC1	0.14	-0.02	0.60	0.31	0.08	0.00	-0.1	-0.35	-0.22	-0.20	-0.25
PC2	-0.18	-0.18	-0.01	0.20	0.09	-0.08	-0.15	-0.15	-0.18	-0.07	0.15
PC3	0.67	0.60	-0.35	-0.42	0.64	0.60	-0.35	-0.49	-0.47	0.42	0.67
PC4	-0.13	-0.34	-0.04	0.19	-0.20	-0.14	0.15	0.03	0.16	0.03	0.24
$d_{med(S)}$	0.48		0.22	-0.48	0.38	0.48	-0.12	-0.25	-0.18		

Table 2. Spectral optical properties of the "brown" aerosol in the visible range: AAE, SSA, and SAE (expressed as mean±standard deviation and variation range [minimum- maximum value]), and real and imaginary part (k_λ) of the complex refractive index (RI [λ]).

$AAE_{467-660}$	SSA_{530}	$SAE_{467-660}$	RI_λ		
			real part	k_λ	[λ]
3.5±0.8 [2.5-6]	0.97±0.01 [0.92-0.99]	0.8±0.3 [0-2]	1.460±0.01	$1.2 \cdot 10^{-2}$ ±0.001	[467nm]
			1.454±0.01	$8.0 \cdot 10^{-3}$ ±0.001	[530nm]
			1.512±0.01	$7.5 \cdot 10^{-3}$ ±0.001	[660nm]

FIGURES

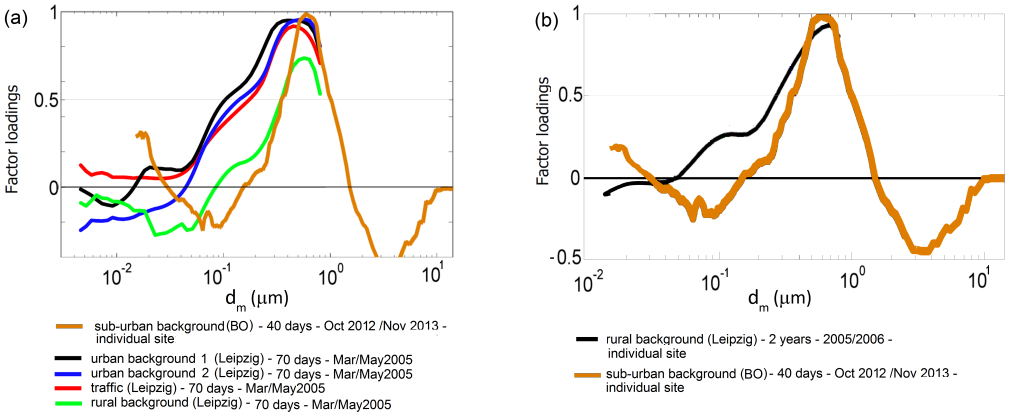

Figure 1. The "droplet" mode of the particle number size distribution (PNSD). Factor loadings calculated by PNSD Principal Component Aanalysis (PCA) are plotted against electrical mobility particle diameter (d_m). Factor loadings are PCA statistical variables indicating correlations between PNSDs and the droplet mode PCA component. Data from this study (brown line) are compared with data obtained by Costabile et al. (2009) in Leipzig (Germany) at: (a) combined urban sites for 70 days in Spring 2005 (green, blue, red, and black lines, as indicated in the legend), and (b) a single site from long-term (2 years) measurements (black line).

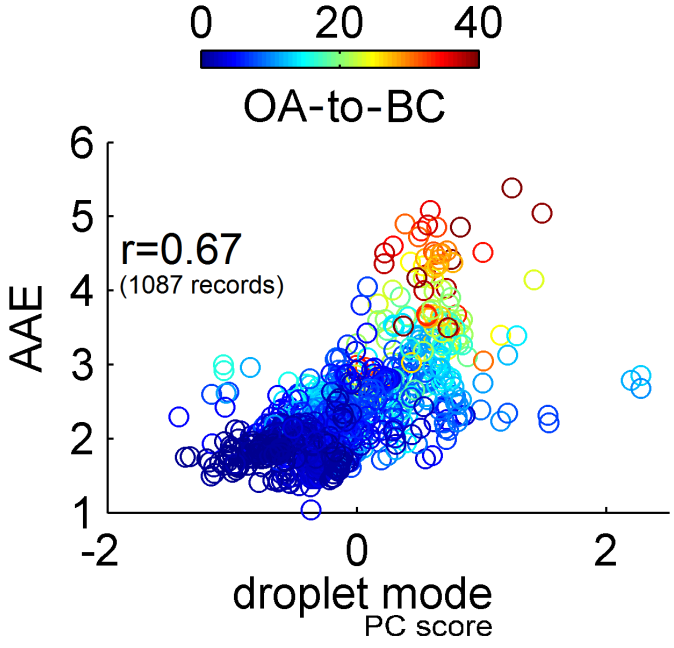

Figure 2. Correlation plot between Absorption Ångström Exponent at 467-660 nm (AAE), and the "droplet mode" aerosol (x-axis is the score of the principal component (PC) representing the droplet mode aerosol). Data color is the Organic Aerosol to Black Carbon ratio (OA-to-BC). The Pearson's correlation coefficient (r) is indicated.

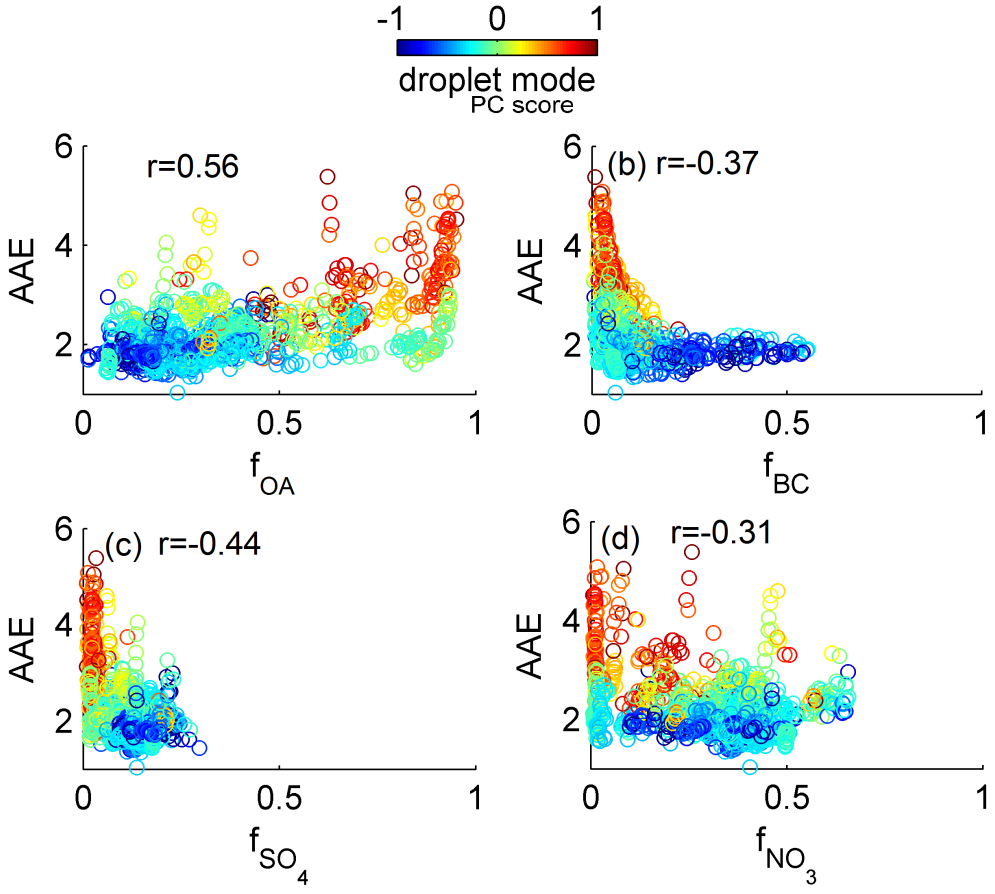

Figure 3. Correlation plots between Absorption Ångström Exponent at 467-660 nm (AAE), and mass fractions of (a) organic aerosol (f_{OA}), (b) Black Carbon (f_{BC}), (c) sulfate (f_{SO_4}), and (d) nitrate (f_{NO_3}). Data color is the score of the droplet mode aerosol. Relevant Pearson's correlation coefficients (r) are indicated.

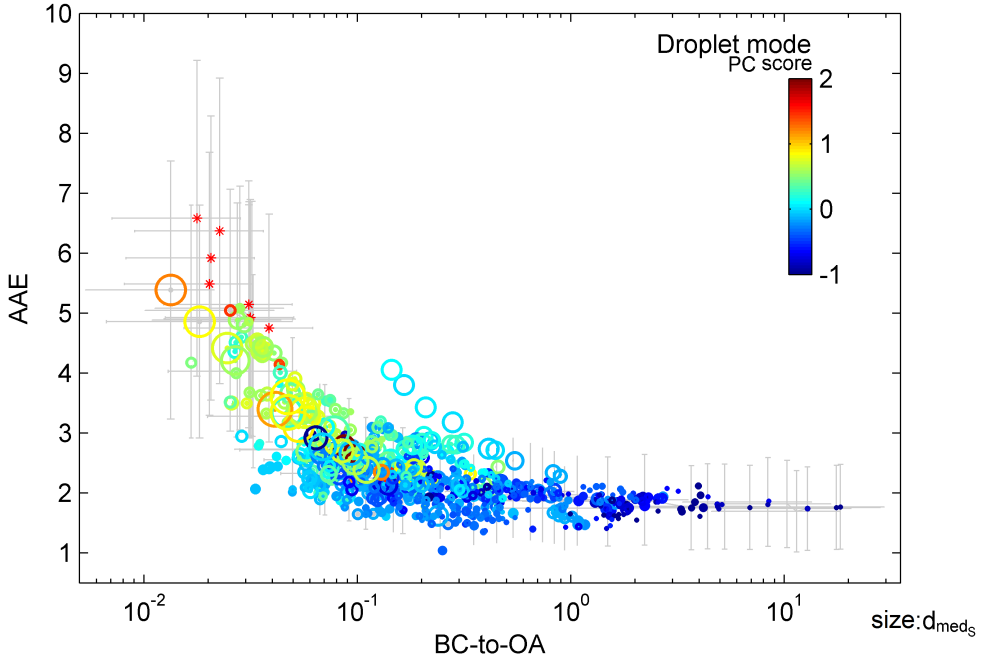

Figure 4. Relation between "brown aerosol" and Black Carbon (BC) to Organic Aerosol (OA) ratio (BC-to-OA). Absorption Ångström Exponent at 467-660 nm (AAE) is plotted against BC-to-OA. Data color is the score of the droplet mode PC extracted by the statistical analysis. Data size is the median diameter of the particle surface size distribution ($d_{med(S)}$). Data indicated by "*" show case-study values illustrated in Fig. 5. Grey bars indicate measurement uncertainty.

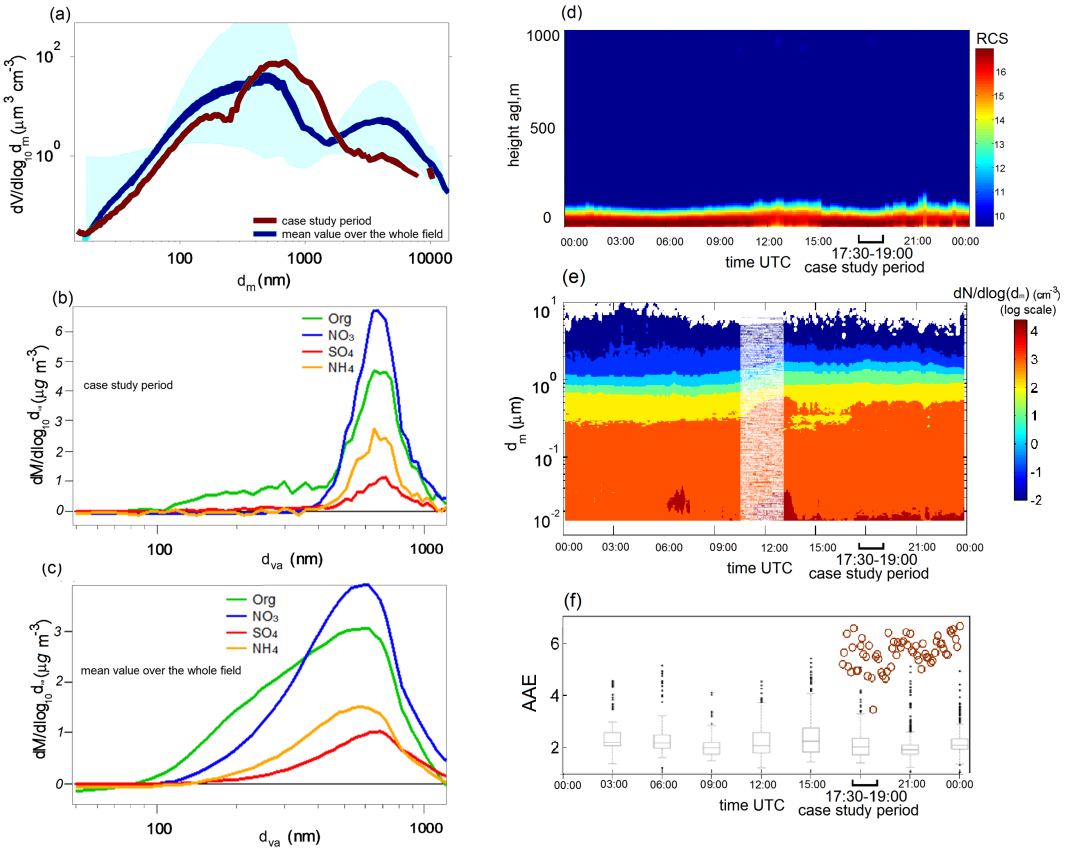

Figure 5. A case-study illustrating major features of the "brown aerosol". Case-study period is the first of February,2013, from 17:30 to 19:00 UTC. Case-study values are compared with mean values over the whole field experiment. Panels illustrate: (a) particle volume size distribution ($dV/dlog_{10}d_m$, based on electrical mobility particle diameter d_m) during the case-study and relevant mean values; (b) particle mass size distribution ($dM/dlog_{10}d_{va}$, based on vacuum aerodynamic diameter, d_{va}) during the case-study, and (c) relevant mean values; (d) aerosol vertical profiles in the atmosphere during the case-study day (time-height cross section of the range corrected signal, RCS=ln(S$\times R^2$), from a LD40 ceilometer); (e) particle number size distributions during the case-study day (whiter area includes corrupted data); (f) Absorption Ångström Exponent at 467-660 nm (AAE) during the case study day (brown circles), and relevant statistical values during the whole field (grey box plots, showing median, percentiles, and outliers).

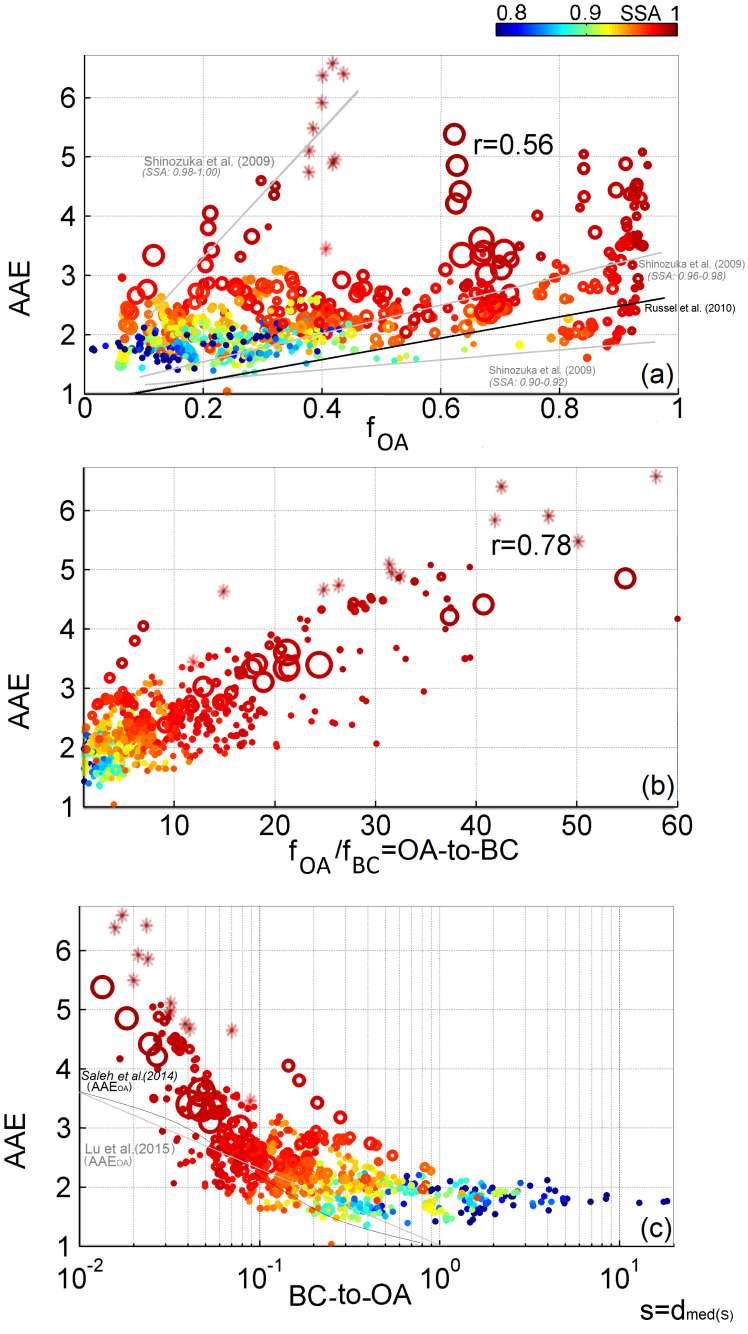

Figure 6. Dependence of Absorption Ångström Exponent at 467-660 nm (AAE) on (a) organic aerosol mass fraction (f_{OA}), (b) Organic Aerosol (OA) to Black Carbon (BC) ratio (OA-to-BC), and (c) BC-to-OA ratio. Data color is Single Scattering Albedo at 530 nm. Data size is median diameter of particle surface size distributions (d_{med_S}, ranging from 50 to 300 nm). Data indicated by "*" show case study values illustrated in Fig. 5. Relevant Pearson's correlation coefficients (r) are indicated. For comparison, we show previous results: (a) by Russell et al. (2010) (black line) and Shinozuka et al (2009) (grey lines, for the SSA bins of 0.90-0.92, 0.96-0.98 and 0.98-1.00) ; (c) by Saleh et al. (2014) (black line), and Lu et al. (2015) (grey line). Note that AAE includes contributions from both BC and OA, whereas in panel (c), Lu et al. (2015) and Saleh et al. (2014)'s results refer to AAE_{OA} only.

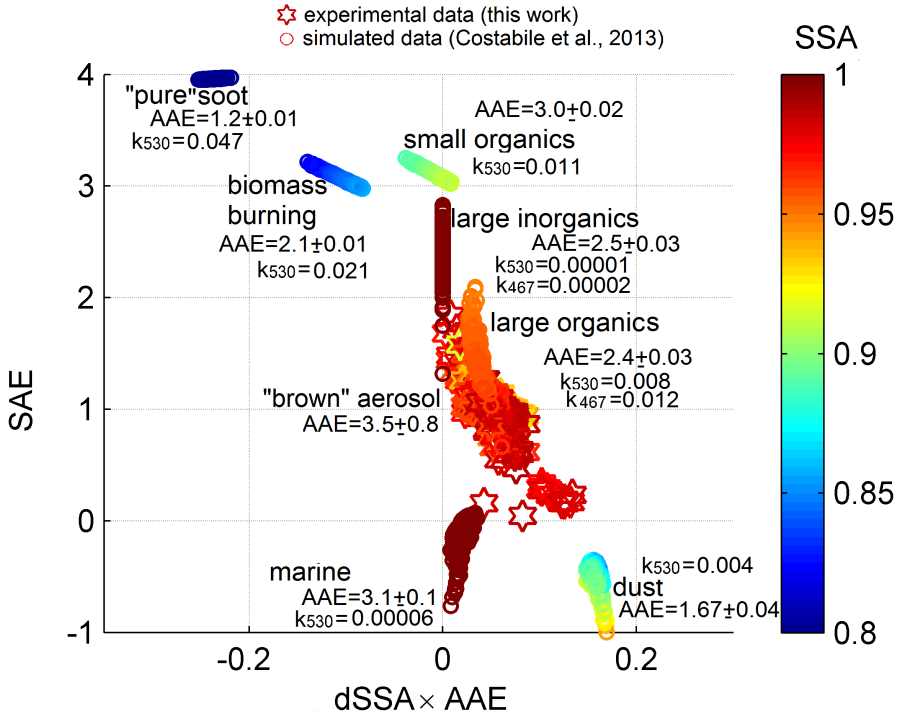

Figure 7. Optical signature of the "brown aerosol" as indicated by the paradigm proposed by Costabile et al. (2013). Absorption Ångström Exponent at 467-660 nm (AAE) times spectral variation of Single Scattering Albedo from 660 to 467 nm (dSSA = SSA_{660} - SSA_{467}) is plotted against Scattering Ångström Exponent at 467-660 nm (SAE). Panel (a) shows experimental data of the droplet mode obtained in this work (representing the brown aerosol) in comparison with key aerosol types obtained through Mie simulations. Data color is SSA at 520 nm. Relevant AAE values for key aerosol types are indicated as mean±standard deviation. Panel (b) zooms in panel a to show the "brown" aerosol optical properties variability with varying major PM_1 mass fractions (f_{OA}, f_{BC}, f_{SO_4}, f_{NO_3}).

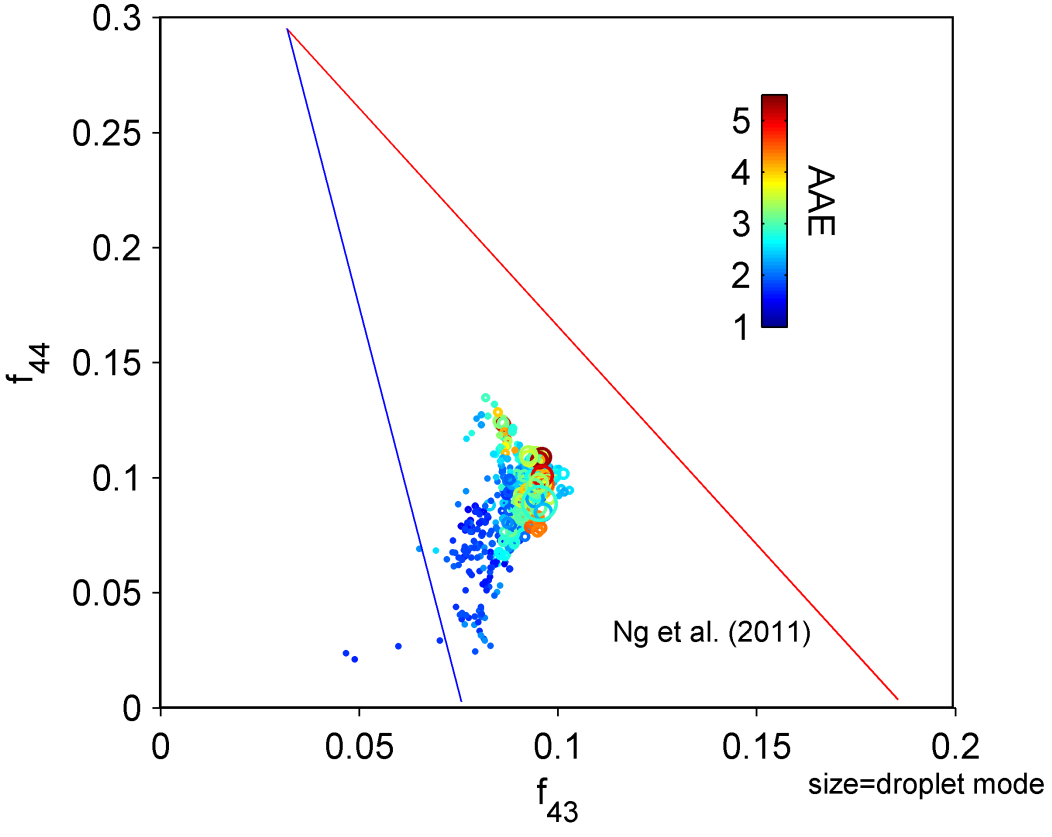

Figure 8. "Triangle plot" reproduced from Ng et al. (2011) for the "brown" aerosol. f_{44} is plotted against f_{43}, data color being the Absorption Ångström Exponent at 467-660 nm (AAE), and data size the droplet mode score. The triangular space indicated by red and blue lines shows where the majority of OA values measured in ambient samples fall into.